

ROBUST LINE-BASED CALIBRATION OF LENS DISTORTION FROM A SINGLE VIEW

Thorsten Thormählen, Hellward Broszio, Ingolf Wassermann

thormae@tnt.uni-hannover.de

University of Hannover, Information Technology Laboratory, Hannover, Germany

ABSTRACT

Line-based camera calibration methods estimate the radial lens distortion from a single view. They use only the constraint, that straight lines in the 3D world must project to straight lines in the image plane, if the distortion is compensated. Therefore neither calibration pattern nor information about other camera parameters are necessary. Former approaches are impaired by real curved lines in the 3D world, that are interpreted as straight lines. This affects their robustness and reduces the accuracy of the estimation. The problem is solved in this paper by a novel efficient outlier elimination of real curved lines in the 3D world. The given results show the significant improvement of robustness and accuracy of the calibration by the applied outlier elimination.

1. INTRODUCTION

Camera calibration is a basic technology for computer vision tasks. Usually, a mathematical parameter model of a pinhole camera with perspective projection is used to describe the mapping between the 3D world and the 2D camera image. Using homogeneous coordinates, the mapping function of the pinhole camera is a simple linear equation system. If low-cost or wide-angle lens systems are used, the linear pinhole camera model fails. In this case the radial lens distortion is the dominating source of mapping errors. It is necessary to compensate this distortion by a non-linear inverse radial distortion function. It corrects measurements in the 2D camera image to those that would have been obtained with a linear pinhole camera model.

Most camera calibration methods estimate simultaneously the inverse radial distortion function and the parameters of the linear pinhole camera model.

Therefore, classical camera calibration methods use calibration patterns or reference objects with known 3D structure [1, 2]. Thus, they can solve the calibration problem by establishing control points of which true coordinates are known, both in the 2D camera image and the 3D world. In practice, however, it is often necessary to perform computer vision tasks on images already recorded without any calibration object.

Auto-calibration methods do not require a calibration object but must be applied on multiple views taken by a moving or rotating camera and not on a single view. Some

of them, which also take radial distortion into account [3, 4, 5], first estimate the parameters of the linear pinhole camera model and then reduce the residual error of their cost function by applying the inverse radial distortion function.

The estimated inverse radial distortion function depends on the parameters of the linear pinhole camera model. Thus, estimation errors of these parameters propagate to errors in the inverse radial distortion function.

In contrast, line-based approaches like [6, 7, 8, 9] need no calibration object and can estimate the radial lens distortion separately from the parameters of the linear pinhole camera model. They obtain the inverse radial distortion function from just one camera view by using the constraint that straight lines in the 3D world must always project to straight lines in the 2D image plane under any perspective projection. From this constraint it follows that the observed curvature of projected straight lines are caused by radial lens distortion. Thus a correct inverse radial distortion function is found if it maps all curved lines into straight lines. The only precondition for line-based approaches is that the 3D scene contains straight 3D lines, which is valid for most man-made environments.

In this paper a line-based approach to calibrate radial lens distortion is presented. In contrast to other line-based approaches a highly efficient outlier elimination of those curved lines in the 2D image plane is performed, that do not correspond to straight lines in the 3D scene. By statistical analysis of the estimation results with and without outlier elimination, it will be shown, that line-based approaches must apply an outlier elimination to achieve robustness and to increase accuracy of the estimation.

The following section contains a short introduction to the source of radial lens distortion and derives a parameterisation for the inverse radial distortion function. In Section 3 the new line-based calibration method with efficient outlier elimination is described. Section 4 compares results with and without outlier elimination. The paper ends with a conclusion.

2. INVERSE RADIAL DISTORTION FUNCTION

In real camera systems, especially if wide-angle lenses are used, the assumption of a linear pinhole camera model is not valid. If a lens and an aperture ring are added to the mathematical camera model the source of radial lens distortion can be explained.

Due to the lens, the location of a sharp projection of the 3D scene point \mathbf{P} does not lie in the image plane, but in a point \mathbf{p} located in front of the plane, as shown in Fig. 1. The corresponding point in the image plane $\mathbf{p}_u = (x_u, y_u)^\top$ is the center of the circle of confusion of \mathbf{P} . For a sharper projection, the circle of confusion is reduced by a smaller lens aperture. As illustrated in Fig. 1 the smaller

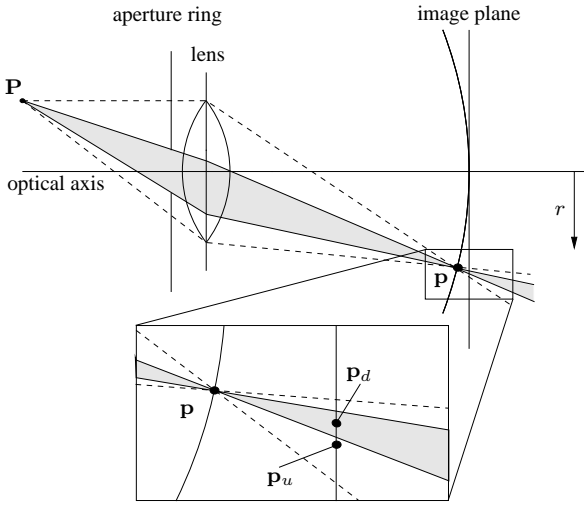


Figure 1: Source of radial lens distortion.

aperture causes not only a smaller circle of confusion but also moves the center of the circle from the undistorted point \mathbf{p}_u to the distorted point $\mathbf{p}_d = (x_d, y_d)^\top$. If the aperture ring is in front of the lens, as shown in Fig. 1, the result is a barrel distortion. An aperture ring behind the lens causes a pincushion distortion. Both kinds of radial lens distortion are illustrated in Fig. 2.

The inverse radial distortion function is the mapping from the distorted point \mathbf{p}_d to the undistorted point \mathbf{p}_u . It can be concluded from the location of the point of sharp projection \mathbf{p} that the radial distortion increases with the radius r . Thus, the inverse radial distortion function $f(r_d)$ can be approximated and parameterised by the following Taylor expansion:

$$r_u = f(r_d) = r_d + r_d \sum_{i=0}^{\infty} \kappa_i r_d^{i-1} \quad (1)$$

with

$$r_u = \sqrt{x_u^2 + y_u^2} \quad \text{and} \quad r_d = \sqrt{x_d^2 + y_d^2}$$

it follows that

$$x_u = x_d + x_d \sum_{i=0}^{\infty} \kappa_i r_d^{i-1} \quad (2)$$

$$y_u = y_d + y_d \sum_{i=0}^{\infty} \kappa_i r_d^{i-1} \quad (3)$$

Practical tests have shown, that it is sufficient to take only the parameters κ_3 and κ_5 into account. Using more parameters brings no major improvement to the approximation of $f(r_d)$ for images in video resolution. In addition an estimation of less parameters is more robust. Thus, we simplify Eq. (2) and Eq. (3) to:

$$x_u = x_d + x_d(\kappa_3 r_d^2 + \kappa_5 r_d^4) \quad (4)$$

$$y_u = y_d + y_d(\kappa_3 r_d^2 + \kappa_5 r_d^4). \quad (5)$$

The parameter κ_3 has the dominant influence on the kind of radial lens distortion. If $\kappa_3 > 0$, a barrel distortion and if $\kappa_3 < 0$, a pincushion distortion is compensated by $f(r_d)$ (see Fig. 2).

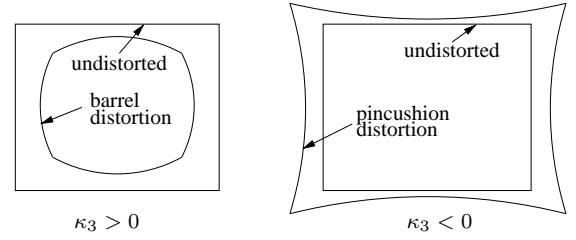


Figure 2: Barrel and pincushion distortion.

3. CALIBRATION OF LENS DISTORTION

The calibration process can be divided into four steps:

- Detection of points on curved line segments
- Linkage of curved line segments
- Outlier elimination
- Final parameter estimation of the inverse radial distortion function

3.1. Detection of points on curved line segments

The presented calibration method relies on the constraint, that straight lines in the 3D world must always project to straight lines in the 2D image plane, if the radial lens distortion is compensated. Thus, with radial lens distortion a point \mathbf{P} on a straight lines in the 3D world is projected to a distorted point \mathbf{p}_d on a curved line. Therefore we search for an inverse radial distortion function $f(r_d)$, that maps

all points \mathbf{p}_d on curved lines into points \mathbf{p}_u on straight lines. So in a first step the points \mathbf{p}_d on curved lines are detected.

Points \mathbf{p}_d on curved lines can be found with a straight line detector, which seems contradictory at first sight. But by increasing the tolerance region of the straight line detector, segments of curved lines are detected as straight lines, as shown in Fig. 3.

The straight line detector is not described here because such algorithms can be taken from literature, provided that the coordinates of the points \mathbf{p}_d on the curved line segments are detected with subpixel accuracy.

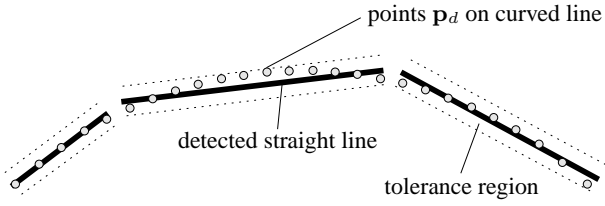


Figure 3: Detection of points \mathbf{p}_d on curved line segments with a straight line detector.

3.2. Linkage of curved line segments

The inverse radial distortion function $f(r_d)$ will be estimated from only one line in the outlier elimination step utilizing the difference between a straight line and a curved line. If the curved line is short, this difference is small (see left line in Fig. 3), and the estimation is very sensitive to noise. Thus, using long lines increase the robustness of the estimation.

To provide long curved lines, the detected straight line segments from the previous step must be linked. It is assumed that two line segments belong together, if they have nearly the same direction and their endpoints are sufficiently close together. The link algorithm searches within a radius R around each endpoint for endpoints of other lines. Consequently, in the example given in Fig. 4, the endpoints of line 2 and 3 are valid candidates because their distance ρ to the endpoint of line 1 is smaller than R . Then the algorithm checks if the lines run in the same direction by checking if the absolute value of the angle α is smaller than a certain threshold.

To suppress the linkage of parallel lines, a last check is performed, which demands that the endpoint of the linked line has a perpendicular distance d to the other line smaller than the threshold D . Therefore, the endpoint of a linked line can only be located in the gray area marked in Fig. 4.

Finally, all short lines and all lines in radial direction are removed, because they contain no reliable information about the radial lens distortion. The result is a set of M long

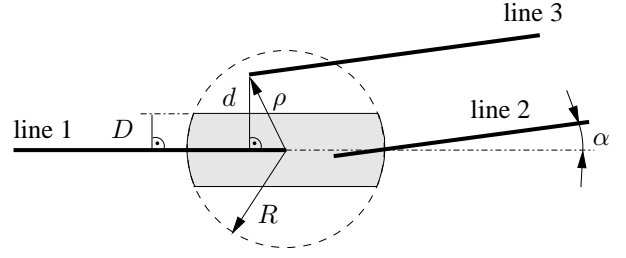


Figure 4: Linkage of straight lines, which represent segments of curved lines. The connection of line 2 and line 1 is valid. The endpoint of line 3 is not located in the gray area and therefore line 3 is not linked.

curved lines L_m with $m = 1, \dots, M$, where every line consists of N_m distorted points $\mathbf{p}_{d,n}$ with $n = 1, \dots, N_m$.

3.3. Outlier elimination

In order to establish a robust estimation only straight lines in the 3D world should be used for estimation of the inverse radial distortion function $f(r_d)$. So curved lines in the 3D world must be detected and eliminated from the set of long curved lines.

The outlier elimination applies the Random Sample Consensus (RANSAC) technique [10]. RANSAC is an approved technique for outlier elimination and is used for many applications in the field of computer vision. The advantage of this technique is, that it can cope with larger numbers of outliers compared to other techniques.

The application of the RANSAC starts with the random selection of one long curved line L_m out of the set. The inverse radial distortion function $f(r_d)$ is estimated from this curved line. Therefore, in the following a cost function for the estimation of the parameters κ_3 and κ_5 of the inverse radial distortion function from one long curved line is derived.

With Eq. (4) and Eq. (5) all N_m distorted points $\mathbf{p}_{d,n} = (x_{d,n}, y_{d,n})^\top$ of the selected long curved line are mapped to the undistorted points $\mathbf{p}_{u,n} = (x_{u,n}, y_{u,n})^\top$ by

$$x_{u,n} = x_{d,n} + x_{d,n}(\kappa_3 r_{d,n}^2 + \kappa_5 r_{d,n}^4) \quad (6)$$

$$y_{u,n} = y_{d,n} + y_{d,n}(\kappa_3 r_{d,n}^2 + \kappa_5 r_{d,n}^4) \quad (7)$$

All N_m undistorted points $\mathbf{p}_{u,n}$ should now lie on a straight line. Thus, an associated straight line Λ_m through $\mathbf{p}_{u,n}$ is estimated using linear regression. If Λ_m is represented in Hesse's normal form, it has three unknowns n_x , n_y and d_0 :

$$\Lambda_m : \begin{pmatrix} n_x \\ n_y \end{pmatrix}^\top \begin{pmatrix} x \\ y \end{pmatrix} - d_0 = 0 \quad (8)$$

To determine these unknowns with linear regression, the following expressions are calculated:

$$\begin{aligned} E_x &= \frac{1}{N_m} \sum_{n=1}^{N_m} x_{u,n} & E_y &= \frac{1}{N_m} \sum_{n=1}^{N_m} y_{u,n} \\ E_{xx} &= \frac{1}{N_m} \sum_{n=1}^{N_m} (x_{u,n})^2 & E_{yy} &= \frac{1}{N_m} \sum_{n=1}^{N_m} (y_{u,n})^2 \\ E_{xy} &= \frac{1}{N_m} \sum_{n=1}^{N_m} x_{u,n} y_{u,n} \end{aligned}$$

Two cases have to be distinguished:

If $E_{xx} - (E_x)^2 \geq E_{yy} - (E_y)^2$, the associated straight line Λ_m is parameterized as

$$\Lambda_m : \quad y = ax + b \quad (9)$$

with

$$a = \frac{E_{xy} - E_x E_y}{E_{xx} - (E_x)^2} \quad b = \frac{E_{xx} E_y - E_x E_{xy}}{E_{xx} - (E_x)^2} \quad (10)$$

the three unknowns follows as

$$n_x = \frac{-a}{\sqrt{a^2+1}} \quad n_y = \frac{1}{\sqrt{a^2+1}} \quad d_0 = \frac{b}{\sqrt{a^2+1}} \quad (11)$$

It is not possible to describe a straight line parallel to the y -axes with Eq. (9). Thus in the second case, if $E_{xx} - (E_x)^2 < E_{yy} - (E_y)^2$, the parameterization of the associated straight line Λ_m changes to:

$$\Lambda_m : \quad x = cy + d \quad (12)$$

with

$$c = \frac{E_{xy} - E_x E_y}{E_{yy} - (E_y)^2} \quad d = \frac{E_{yy} E_x - E_y E_{xy}}{E_{yy} - (E_y)^2} \quad (13)$$

In this case the three unknowns of Eq. (8) are

$$n_x = \frac{1}{\sqrt{c^2+1}} \quad n_y = \frac{-c}{\sqrt{c^2+1}} \quad d_0 = \frac{d}{\sqrt{c^2+1}} \quad (14)$$

Now an associated straight line Λ_m is found, which is a function of κ_3 , κ_5 and the points $\mathbf{p}_{d,n}$. If a correct solution for κ_3 and κ_5 is found, all N_m undistorted points $\mathbf{p}_{u,n}$ should lie on that straight line (see Fig. 5) and therefore fulfill Eq. (8).

Thus, a cost function with the residual errors ϵ_n of Eq. (8) is formulated as:

$$\epsilon_n = \begin{pmatrix} n_x \\ n_y \end{pmatrix}^\top \begin{pmatrix} x_{u,n} \\ y_{u,n} \end{pmatrix} - d_0 \quad (15)$$

$$\sum_{n=1}^{N_m} (\epsilon_n)^2 \longrightarrow \min \quad (16)$$

This cost function is a non-linear function of κ_3 , κ_5 and the points $\mathbf{p}_{d,n}$ of one long curved line L_m . To estimate

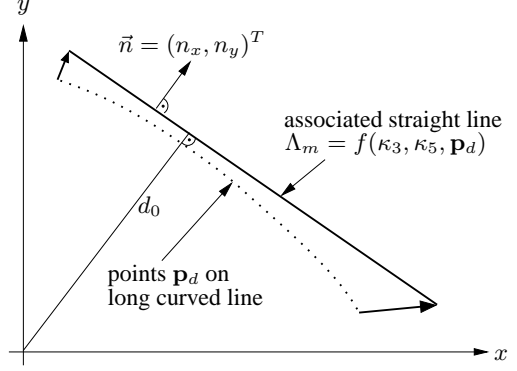


Figure 5: Points \mathbf{p}_d on a curved line are mapped on points \mathbf{p}_u on the associated straight line Λ_m , which is a function of κ_3 , κ_5 and the points \mathbf{p}_d .

κ_3 and κ_5 , the sum of squares is minimized using the iterative Levenberg-Marquardt method [11]. Because nothing is known about the sign of the parameters, the initial values of κ_3 and κ_5 are set to zero.

The RANSAC method estimates the actual parameters κ_3 and κ_5 from a randomly chosen curved line L_m out of the set. Then it tries to compensate the radial distortion with these actual parameters and evaluates the percentage of outliers. A line L_m is considered as outlier, if more than a certain percentage of its undistorted points $\mathbf{p}_{u,n}$ have an absolute deviation larger than δ_{\max} from its associated straight line. The absolute deviation can be calculated with Eq. (15) using the actual parameters κ_3 and κ_5 . If the actual parameters generate too many outliers, a new curved line L_m is randomly chosen until a satisfying solution for the parameters κ_3 and κ_5 is found. The curved lines, which support the satisfying solution, are called inliers. Only the I long curved lines L_i with $i = 1, \dots, I$, which are detected as inliers, are applied to estimate the final parameters as described in the following processing step.

3.4. Final parameter estimation

The final parameter estimation of the inverse radial distortion function $f(r_d)$ minimizes the cost function

$$\sum_{i=1}^I \sum_{n=1}^{N_m} (\epsilon_n)^2 \longrightarrow \min \quad (17)$$

This cost function is a non-linear function of κ_3 , κ_5 and the points $\mathbf{p}_{d,n}$ of all long curved inlier lines L_i . Again, the cost function is minimized with the Levenberg-Marquardt method. As initial values for κ_3 and κ_5 the best parameter set from the outlier elimination is used.

4. RESULTS

4.1. Synthetic images

The improvement of robustness and accuracy is tested on synthetic images by applying an efficient outlier elimination before the final parameter estimation.

An example for a synthetic image is given in Fig. 10. It contains straight lines as well as curved lines in the 3D world. For this image the ground truth parameters of the inverse radial distortion function are $\kappa_3 = 1.0 \cdot 10^{-4} \text{mm}^{-2}$ and $\kappa_5 = 0.0 \text{mm}^{-4}$. In the synthetic image, 64 long curved lines L_m are detected. The outlier elimination step detects 21 long curved outlier lines and thus 43 inlier lines L_i are used for final parameter estimation, which gives a result of $\kappa_3 = 0.9968 \cdot 10^{-4} \text{mm}^{-2}$ and $\kappa_5 = 5.316 \cdot 10^{-10} \text{mm}^{-4}$. The estimation error results in a maximum deviation of $\Delta r = 0.9381$ pixel at the corners of the image. Fig. 11 shows the undistorted image after application of the estimated inverse radial lens distortion function. Inlier lines L_i are marked green and outlier lines are red.

Fig. 6 and Fig. 7 compare the accuracy of the estimation result without and with outlier elimination. For simplicity only the parameter κ_3 is taken into account. In this experiment the parameter κ_3 is estimated only from a single line. Fig. 6 shows the result of the estimation of κ_3 without outlier elimination, where the relative frequency over κ_3 for 64 long curved lines L_m is plotted. It is obvious, that these 64 lines contain outliers, because the relative frequency of κ_3 is distributed over a wide range, which can not be explained with noisy measurement of the distorted points p_d . Consequently, the final parameter estimation without outlier elimination gives a worse result of $\kappa_3 = 0.8732 \cdot 10^{-4} \text{mm}^{-2}$ and $\kappa_5 = 4.234 \cdot 10^{-10} \text{mm}^{-4}$. The higher estimation error without outlier elimination results in a higher maximum deviation of $\Delta r = -12.135$ pixel at the corners of the image.

In contrast, if outlier elimination is applied, the estimation result is remarkable better. In Fig. 7 the parameter κ_3 is estimated separately from each of the 43 long curved lines L_i , which are detected as inliers. The relative frequency of κ_3 is distributed over a smaller range around the true value for κ_3 . Thus, it is shown that the outlier elimination leads to the improvement of the estimation accuracy in this example.

The next experiment evaluates the improvement of robustness. The presented method is applied on 100 images out of a synthetic image sequence showing different areas of a 3D scene. Again the ground truth parameters of the inverse radial distortion function is $\kappa_3 = 1.0 \cdot 10^{-4} \text{mm}^{-2}$. Fig. 8 and Fig. 9 show the relative frequency of the parameter κ_3 after final parameter estimation. Robustness of the algorithm with and without outlier elimination is

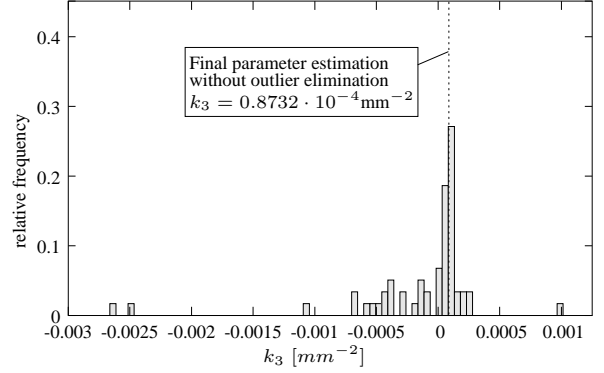


Figure 6: Relative frequency of the parameter κ_3 using single lines L_m for estimation. Outliers and inliers are evaluated.

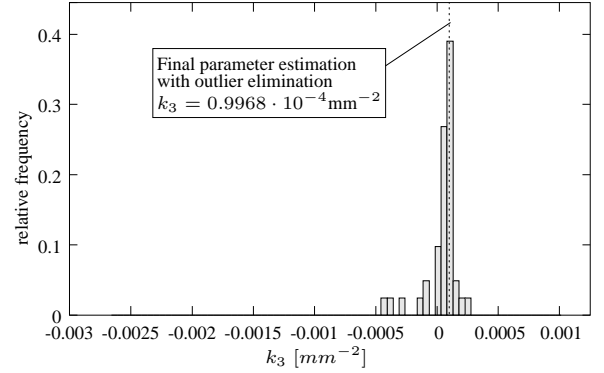


Figure 7: Relative frequency of the parameter κ_3 using single lines L_i for estimation. Only inliers are evaluated.

measured by the percentage of performed estimations of κ_3 with an estimation error, that results in a deviation of less than one pixel in the distortion compensated images. Because the deviation of image points caused by an estimation error increases with the image radius r , the deviation is evaluated for image points, that are located at the half of the maximum radius.

If an outlier elimination is applied the robustness is 94% in contrast to 33% without outlier elimination. Because both algorithms are applied on the same noisy measurement of the distorted points p_d , it can be concluded, that the outlier elimination increases the robustness significantly and therefore it is a necessary step for line-based calibration methods.

4.2. Natural images

Natural images are used to compare the presented line-based approach with Tsai's calibration method [1], which uses a calibration pattern. In Fig. 12 the original distorted image is shown. In Fig. 13 and Fig. 14 the result of Tsai's

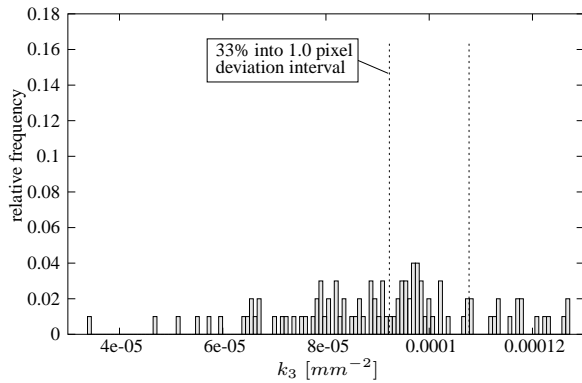


Figure 8: *Relative frequency of the parameter κ_3 applying final parameter estimation on 100 images without outlier elimination.*

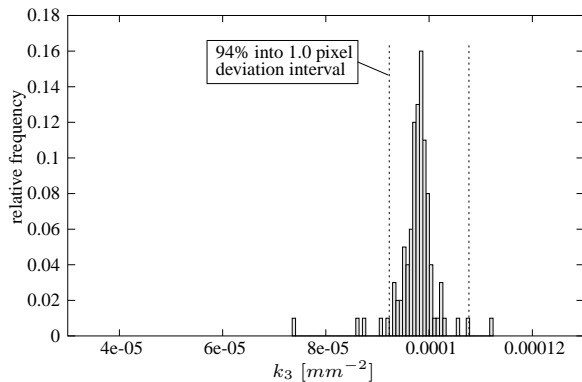


Figure 9: *Improved robustness: Relative frequency of the parameter κ_3 applying final parameter estimation on 100 images with outlier elimination step.*

calibration method and the result of the line-based approach are opposed. By inspection of the straight lines there is no quality difference visible. Other examples of tested natural images are given in Fig. 15 and Fig. 17, which are two images out of a sequence taken with a low-cost internet camera, which produces large lens distortion and blur. Fig. 16 and Fig. 18 show the undistorted images.

5. CONCLUSIONS

Automatic line-based calibration methods are especially suitable for images taken in man-made environments, because here the precondition of straight lines in the 3D world is valid. In these cases the method is comfortable to use, because it does not require any calibration pattern. In contrast to other approaches the described method uses a novel efficient outlier elimination step, which removes curved lines in the 3D world. The experimental results

have shown that the outlier elimination step increases robustness and accuracy significantly.

6. REFERENCES

- [1] R. Y. Tsai, "A versatile camera calibration technique for high-accuracy 3-d machine vision metrology using off-the-shelf cameras and lenses," *IEEE Transaction on Robotics and Automation*, vol. 3, 1987.
- [2] Juyang Weng, Paul Cohen, and Marc Herniou, "Camera calibration with distortion models and accuracy evaluation," *IEEE Transactions on Pattern Analysis and Machine Intelligence*, vol. 14, no. 10, pp. 965–980, Oct. 1992.
- [3] G. P. Stein, "Accurate internal camera calibration using rotation, with analysis of sources of error," in *International Conference on Computer Vision*, 1995, pp. 230–236.
- [4] G. P. Stein, "Lens distortion calibration using point correspondences," in *IEEE Conference on Computer Vision and Pattern Recognition*, 1997, pp. 602–608.
- [5] Harpreet S. Sawhney and Rakesh Kumar, "True multi-image alignment and its application to mosaicing and lens distortion correction," *IEEE Transaction on Pattern Analysis and Machine Intelligence*, vol. 21, no. 3, pp. 235–243, Mar. 1999.
- [6] C. Bräuer-Burchardt and K. Voss, "Automatic lens distortion calibration using single views," *Mustererkennung*, vol. 1, pp. 187–194, 2000.
- [7] C. Bräuer-Burchardt and K. Voss, "A new algorithm to correct fish-eye- and strong wide-angle-lens-distortion from single images," in *IEEE International Conference on Image Processing*, 2001, vol. 1, pp. 225–228.
- [8] Moumen Ahmed and Aly Farag, "Non-metric calibration of camera lens distortion," in *IEEE International Conference on Image Processing*, 2001, vol. 2, pp. 157–160.
- [9] F. Devernay and O. Faugeras, "Straight lines have to be straight," *Machine Vision and Application*, vol. 13, pp. 14–24, 2001.
- [10] R. M. A. Fischler and C. Bolles, "Random sample consensus: A paradigm for model fitting with application to image analysis and automated cartography," *Communications of the ACM*, vol. 24, no. 6, pp. 381–395, 1981.
- [11] W. H. Press and et al., *Numerical Recipes in C, 2nd ed*, Cambridge Univ. Press, 1992.

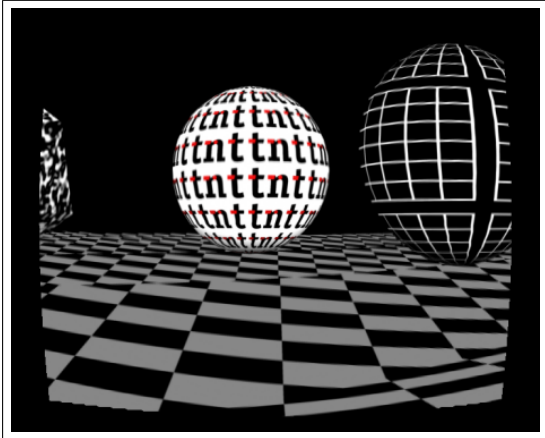


Figure 10: Original synthetic image with ground truth inverse radial distortion function.

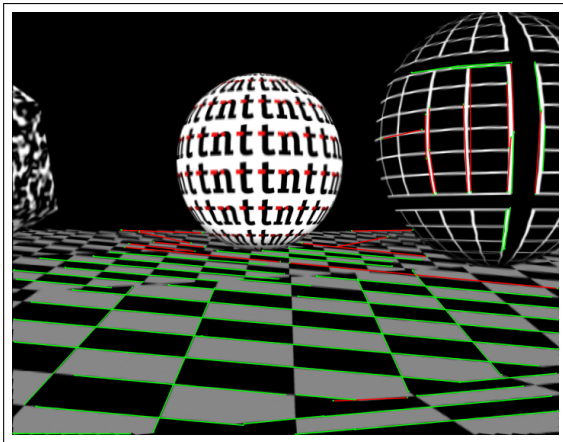


Figure 11: Undistorted synthetic image with outlier elimination (green = inlier, red = outlier).

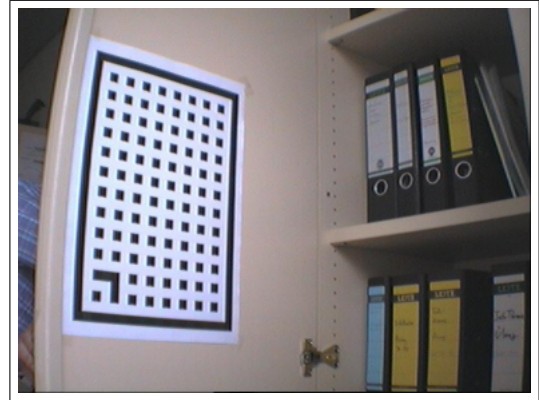


Figure 12: Original image used for comparison with Tsai's camera calibration method.

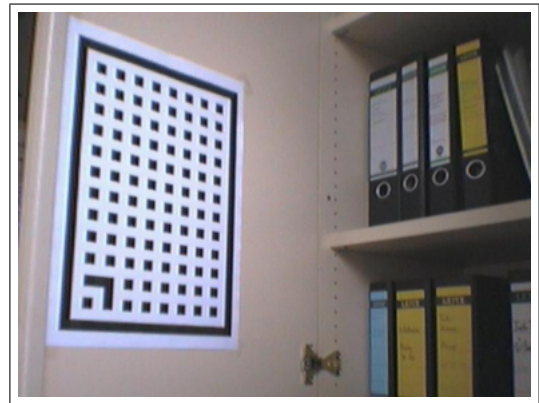


Figure 13: Undistorted image using Tsai's camera calibration method, which uses the calibration pattern.

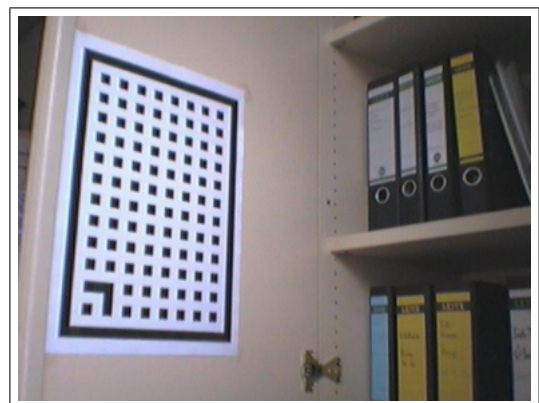


Figure 14: Undistorted image using the presented line-based calibration method. The calibration pattern is not used.



Figure 15: *Original natural image, showing a building of the University of Hannover.*



Figure 17: *Original natural image, showing the garden in front of the building.*



Figure 16: *Undistorted natural image (green = inlier, red = outlier).*

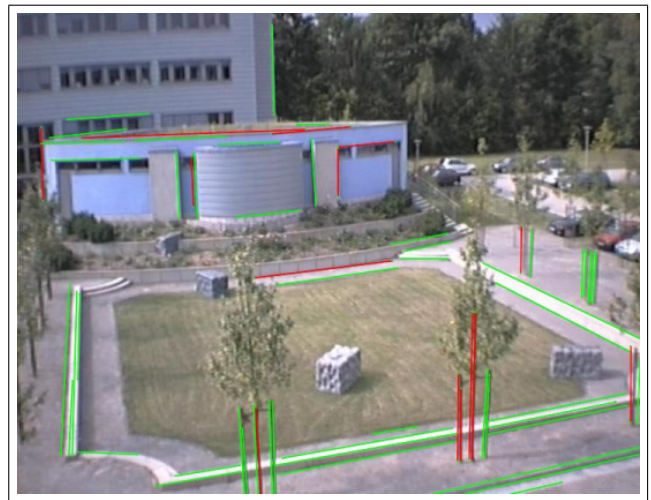


Figure 18: *Undistorted natural image (green = inlier, red = outlier).*